Experimental test of a Doppler spectro-imager devoted to giant-planet seismology and atmospheric dynamics

L. Soulat[1], F.-X. Schmider[1], S. Robbe-Dubois[1], Y. Bresson[1], J.-B. Daban[1], J. Gay[1], C. Gouvret[1], Y. Fantei[1], C. Combier[1], T. Appourchaux[2], G. Morinaud[2], J.C. Leclech[2], J.P. Dubois[2], and P. Gaulme[3,4]

[1] Laboratoire Lagrange, Université de Nice Sophia Antipolis, UMR 7293, Observatoire de la Cote d'Azur (OCA), Nice, France
e-mail: schmider@oca.eu
[2] Institut d'Astrophysique Spatiale, Université Paris XI, UMR 8617, 91405 Orsay Cedex, France
[3] Department of Astronomy, New Mexico State University, P.O. Box 30001, MSC 4500, Las Cruces, NM 88003-8001, USA
[4] Apache Point Observatory, 2001 Apache Point Road, P.O. Box 59, Sunspot, NM 88349, USA

Received <date> / Accepted <date>

ABSTRACT

Context. We present a new instrumental concept that can be applied to the giant planets seismology. The instrument Doppler Seismo Imager (DSI) was proposed in the frame of the JUICE space mission from the ESA Cosmic Vision programme for the study of Jupiter. The science objectives of the proposed were the determination of the internal structure of Jupiter by asteroseismology, i.e. by measurement of the frequencies of acoustic eigenmodes, and the study of the Jovian atmospheric dynamics.
Aims. The concept of the DSI instrument was derived from the SYMPA instrument, that provided the first clear detection of jovian acoustic modes. It is based on a modified Mach-Zehnder interferometer that acts as an imaging Fourier transform spectrometer with a fixed optical path difference in order to produce radial velocity maps of the planet at regular time interval. The operation in space impose constraints on the instrumental in term of power, mass, data transmission rate. We want to check that the instrument could reliably achieve the expected performances in the environment of the mission, taking into account in particular the thermal environment and the effects of radiations.
Methods. The instrumental design was calculated to respond to the scientific requirements, in particular to enable the detection of modes as low as 1 cm/s within the duration of the space mission. In order to estimate real performances and capabilities of operation in spatial environment, a prototype was realized and its properties were measured with a dedicated optical test bench. The prototype instrument was then placed in a thermally controlled vacuum chamber were its behavior was measured in a range of temperature conditions in order to check its thermal stability.
Results. We present here the experimental results obtained on the prototype of the instrument in laboratory to estimate its real performances, and its conformity to theoretical expectations. The conclusion is that the instrument follows most of the requirements and proved to be suitable for the achievement of the initial scientific objectives in the frame of a space mission. It might be used for other applications implying velocity field measurements in solar light.

Key words. Jupiter – asteroseismology – optical instrument – imaging Fourier transform spectrometer – radial velocity – space mission – Cosmic Vision

1. Introduction

The Doppler spectro-imager (DSI) *Echoes* is an instrumental project dedicated to study internal structures and atmospheric dynamics of the giant planets of the Solar system, through radial velocity mapping of a whole planet at the time in the visible domain. Studies of *Echoes* were initially undertaken for *Laplace*, a mission project dedicated to the Jovian system, proposed to the ESA Cosmic Vision program. *Laplace* then turned into the JUpiter ICy moons Explorer (JUICE), which was selected as the first Cosmic Vision "Large" mission. *Echoes* was proposed at the very beginning and was part of the Preliminary Definition Document of *Laplace* to study the formation and evolution of Jupiter's system. Seismology was a first ever objective for a mission devoted to a giant planet, while the study of atmospheric dynamics from radial velocities represented an opportunity to test cloud-tracking wind measurements and a first attempt to directly measure upwelling flows. The design of the instrument has been mainly driven by constraints arising from seismology.

Seismology consists of retrieving the internal density profile of a planet/star from the surface down to the core thanks to measurements of its acoustic mode frequencies (e.g. Jackiewicz et al. 2012). Interiors of giant planets are mostly fluid, and all but Uranus have a deep convective envelope, which makes their seismology much closer to that of solar-like stars rather than telluric planets. Helioseismology has been very successful for the past 40 years to determine the solar internal structure (e.g. Deubner 1975; Christensen-Dalsgaard 2004). The possibility to use seismic technique for Jupiter's internal structure has been envisioned at the very beginning of helioseismology by Vorontsov et al. (1976). Further works have shown how much could be learnt about its interior, in particular the unambiguous determination of the core mass and size (Gudkova & Zharkov 1997). Measurements on the latter would give strong insights on giant planets formation and the Solar System in general, since Jupiter has played a crucial role in shaping the solar system with a large mass and rapid formation. Two scenarii are competing to explain its formation: the nucleated instability model assumes accretion of gas around a several Earth-mass core of rocks and ice (Safronov & Ruskol 1982), while the gravitational instability model proposes that giant planets formed by gravitational collapse from the protoplanetary disk (Cameron 1978; Mayer et al. 2002).

Theoretical works (Vorontsov et al. 1976; Bercovici & Schubert 1987) predict that Jovian global oscillations should have a frequency range of [800, 3500] μHz with 10 to 100 cm s^{-1} amplitude, values that are comparable to the Sun's. Several attempts to observe Jovian global modes have been carried out since the mid-1980s, with thermal infrared photometry (Deming et al. 1989), Doppler spectrometry with magneto-optic (Schmider et al. 1991) and Fourier transform spectrometers (Mosser et al. 1993, 2000), respectively. Infrared observations are affected by atmospheric inhomogeneities and have been unsuccessful so far. In contrast, all of the Doppler measurements exhibit an excess power of about 1 m s^{-2} between 800 and 2000 μHz, which could not be explained by instrumental systematics nor by spurious atmospheric signals. A tentative comb-like structure of 139 ± 3 μHz mean spacing was also identified, but the combination of a low signal-to-noise, the fact that this frequency corresponds to the least common multiple of terrestrial and jovian rotation, and that it was incompatible with theoretical estimates implied that it was probably an artifact.

The need for a specific instrumentation able to combine high spectral and spatial resolution thus emerged from the 1980 and 1990s experiments. The major difficulty of seismic observations of Jupiter is related to its rapid rotation (500 m s^{-1} at the equator on 1 arcsec), which diminishes the instrument's velocity sensitivity and makes it extremely sensitive to pointing errors. The SYMPA instrument is a Fourier tachometer, designed to circumvent this difficulty and whose principle is based on the spectro-imaging of the full planetary disk in a non-scanning mode (Schmider et al. 2007). The optical design is based on a Mach-Zehnder interferometer at fixed optical path difference (OPD). It produces radial velocity maps of Jupiter's upper troposphere by measuring the Doppler shift of solar Mg lines at 517 nm that are reflected by Jupiter's clouds.

Multi-sites ground based observations were obtained with two SYMPA instruments, at San Pedro Martir and Teide Observatories in 2005 (Gaulme et al. 2008), and conducted to the first unambiguous detection of jovian oscillations (Gaulme et al. 2011). The best observation sequence was acquired at Teide and was the only dataset used for science (Gaulme et al. 2011). The analysis of the observations showed evidence of the existence of Jovian oscillations with frequencies compatible to the theoretical models. However, the quality of the observations was limited by the low duty cycle, and also instrumental issues regarding calibration, optical distortions, and thermal drifts. The DSI *Echoes* directly inherits from SYMPA and has been adapted for a space experiment by revisiting the optical design and adding robust calibration procedures. In particular, the working wavelength is changed to maximize contrast and sensitivity of the interference fringes, a particular care is taken to avoid geometric distortions, and the thermal stability is the object of specific control.

In terms of performance for seismology, SYMPA's noise level was about 6 cm $s^{-1}\mu Hz^{-1/2}$, for a 50-h integration time and a 21.5-% duty cycle (Gaulme et al. 2011). All the detected modes were measured with a signal-to-noise ratio (SNR) of about 3. The science team of *Echoes* estimated that modes of amplitude as low as 1 cm s^{-1} should be detected to efficiently constrain Jupiter's internal structure. This represents an increase of instrument performance by a factor 10 with respect to SYMPA. Hence, the noise level in the frequency range surrounding the oscillations, [500, 4000] μHz, must be less than 1 cm s^{-1} $\mu Hz^{-1/2}$. Besides, to allow for unambiguous identification of oscillations in terms of spherical harmonics, *Echoes* needs a duty-cycle larger than 66 % and a frequency resolution lower than 1 μHz, i.e. a run longer than 11.57 days. As regards atmospheric dynamics, the goal of *Echoes* is to reach a sensitivity of 10 m s^{-1} per element of resolution on the planet per hour of integration, and to measure zonal and meridional rotation latitudinal profiles with 1 m s^{-1} of precision in jovian rotation. Another major specificity of *Echoes* with regards to SYMPA is the harsh radiation environment, which influences the choice of materials to build it.

The main purpose of the present work is to propose a design that fits with space requirements and to demonstrates that its technology readiness level (TRL), a scale from 1 to 10 commonly used for qualification of space instruments, to 5. This paper describes *Echoes*'s instrumental concept and the first experimental results obtained on a prototype of the Mach-Zehnder interferometer - core part of the instrument - which was realized at the Observatoire de la Côte d'Azur (OCA). We first describe the measurement principle, i.e. how we extract a radial velocity field from the interference pattern, and the choice of the optimized working spectral domain (Sect. 2). Then, we show how science specifications drive the instrument design, i.e. the pupil size, Mach-Zehnder design, and thermal control (Sect. 3). After a description of the test bench, the experimental testing demonstrates that most of the theoretical performance are met and we suggest minor modifications for the two out-of-specification parameters (Sect. 4). Generally, this experiment validates *Echoes*'s concept, and none element susceptible to compromise operations in space environment is identified.

2. Instrument description

2.1. Measurement principle

The DSI *Echoes* is based on a Mach-Zehnder interferometer with a fixed OPD (see diagram in Fig. 1). Let us consider an electromagnetic wave traveling perpendicularly to the interferometer. A beam splitter, made of two prisms stuck with a semi-reflective coating, splits the incoming light into two beams, which then travel in perpendicular directions. The beam splitter also introduces a $\pi/2$ phase shift between the transmitted and reflected electromagnetic waves, independently from polarization. The two beams propagate in prisms of different refractive indices and thicknesses to introduce an OPD. Thicknesses and refractive indices are chosen such as the OPD generates a π phase shift between the waves traveling in the two arms of the interferometer. In addition to this, a quarter-wave plate is placed in one arm to introduce a $\pi/2$ phase shift between the perpendicular and parallel polarization components of the electromagnetic wave. The two beams then recombine and interfere on another beam splitter. Finally, polarizer cubes separate each output into its perpendicular and parallel components, which leads to four outputs. The four output beams are interfering patterns, quasi-periodic as function of OPD, which phases are in quadrature, i.e. phase-shifted by $k\pi/2$ ($k = 0, 1, 2, 3$). In the ideal case of photometric equipartition and no absorption in the interferometer, the intensity of the

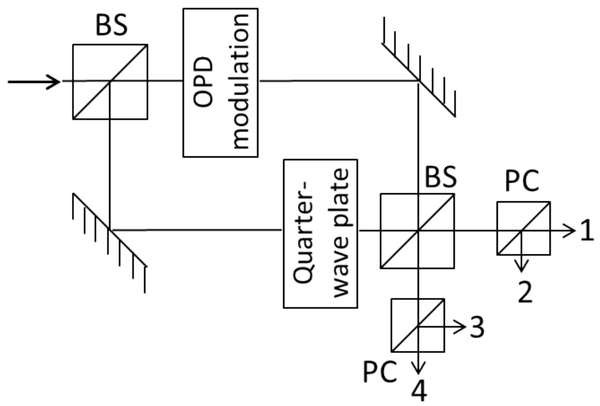

Fig. 1. The modified Mach-Zehnder interferometer, based on two beam splitters (BS), is designed to produce four images in phase quadrature (1,2,3,4). At each output of the Mach-Zehnder, a polarizer cube (PC) divides the beam in two orthogonal linear polarized directions. In one arm, a glass plate is used to modulate the OPD. In the other arm, a quarter-wave plate achieves the phase quadrature.

four interferograms express as:

$$I_1 = \frac{I_0}{4}(1 + \gamma \cos\phi) \quad (1)$$
$$I_2 = \frac{I_0}{4}(1 + \gamma \sin\phi) \quad (2)$$
$$I_3 = \frac{I_0}{4}(1 - \gamma \cos\phi) \quad (3)$$
$$I_4 = \frac{I_0}{4}(1 - \gamma \sin\phi), \quad (4)$$

where I_0 is the incident flux, γ the fringe contrast, and ϕ the fringe phase. The latter expresses as function of the wavenumber σ, the OPD Δ, the radial velocity v_R, and the speed of light c as:

$$\phi = 2\pi\sigma\Delta\left(1 + \frac{v_R}{c}\right). \quad (5)$$

The measurement principle which consists of retrieving the Fourier transform of a optical spectrum from measuring the phase of four interferograms in phase quadrature is known as the ABCD method (see Wyant 1975; Schmider et al. 2007). It is particularly suitable for mapping the radial velocity on each point of an extended object.

The two-by-two combination of the four outputs allows us to cancel the fringe modulation by photometry, and obtain two interferograms U and V in phase quadrature:

$$U = \frac{I_1 - I_3}{I_1 + I_3} = \gamma\cos\phi \quad (6)$$
$$V = \frac{I_2 - I_4}{I_2 + I_4} = \gamma\sin\phi \quad (7)$$

The phase ϕ is simply retrieved by computing the argument of the complex interferogram Z:

$$Z = U + iV = |Z|\, e^{i\phi} \quad (8)$$

Actually, the radial velocity is extracted by computing the argument of Z divided by the complex interferogram Z_{inst}

$$Z_{\text{inst}} = e^{i2\pi\sigma\Delta}, \quad (9)$$

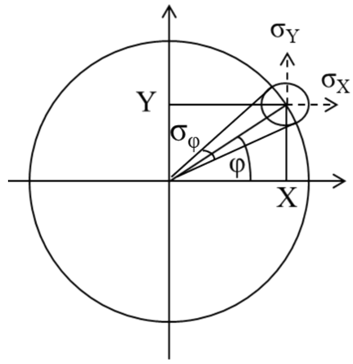

Fig. 2. Standard deviation on the phase determination. **Alonger la caption et refaire la figure avec U et V au lieu de X et Y.**

which corresponds to the instrument's transfer function. In other words, Z_{inst} is the interferogram in absence of radial velocity. Practically, this calibration interferogram is obtained with a spectral lamp, which beams are collimated and reach the Mach-Zehnder in the same way as the astrophysical light.

2.2. Velocity sensitivity

In the ideal case described by Eqs. 1 to 4 , the instrument performance in terms of velocity sensitivity depends on the ability to measure the phase of the fringes. As we show in this section and the following, the optimized performance is a tradeoff between the number of photons and the fringe contrast, which constrains the choice of the spectral domain and the width of the entrance filter. Let us temporary move away from the ideal case by assuming N_i photons on a given point in each image I_i, $i = [1, 4]$. The variance on U and V measurements are the result of the photon noise:

$$\left\langle |\delta U|^2 \right\rangle = \frac{4N_1N_3}{(N_1 + N_3)^3}$$
$$\left\langle |\delta V|^2 \right\rangle = \frac{4N_2N_4}{(N_2 + N_4)^3} \quad (10)$$

The variance of the phase is illustrated in Fig. 2 and expresses as:

$$\left\langle \delta_\phi \right\rangle^2 = \frac{\sin^2\phi \left\langle |\delta U^2| \right\rangle + \cos^2\phi \left\langle |\delta V^2| \right\rangle}{\gamma^2} \quad (11)$$

In the ideal case, $N_i = 0.25N$, the phase variance associated with the photon noise turns to:

$$\left\langle \delta_\phi \right\rangle^2 = \frac{2}{\gamma^2 N} \quad (12)$$

where N is the total number of collected photons. Therefore, the standard deviation on velocity measurements δ_v is:

$$\delta_v = \frac{c\lambda}{\gamma\pi\Delta\sqrt{2N}} \quad (13)$$

This noise level assumes equal transmission for each optical path, a constant and uniform OPD, and a phase quadrature between the four outputs. Any departure from these conditions leads to a lower SNR. The degradation of phase measurement due to transmission unbalance and departure from phase quadrature are treated in Sect. **??** and **??**.

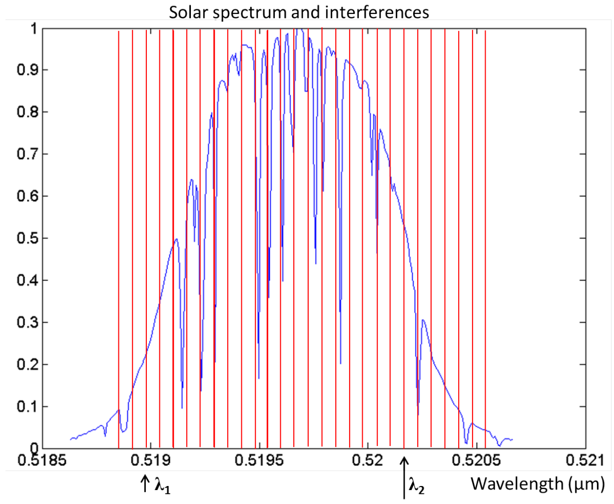

Fig. 3. Interference fringes correspond to solar spectral lines. Fringe contrast is derived from this coherence. **Figure et legende incomprehensibles**

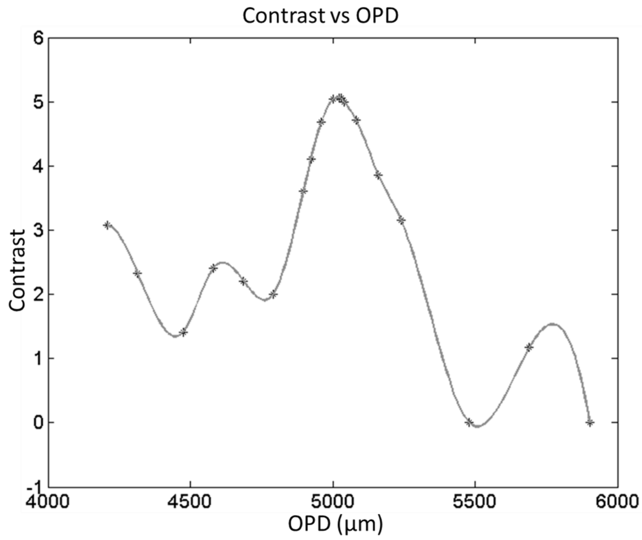

Fig. 4. Fringe contrast as a function of the optical path difference.

2.3. Spectral domain

Echoes is conceived to work with solar spectral lines reflected on Jupiter's top clouds. This choice is motivated by several reasons. Firstly, solar lines are reflected at the top of ammonia clouds, where the optical thickness $\tau = 1$ is reached on an altitude range much smaller than the vertical wavelength of seismic acoustic waves. Secondly, with reflected light, a velocity field at the surface of Jupiter is enhanced by a factor $1 + \cos\alpha$ in terms of Doppler shift, where α is the phase angle (Sun-Jupiter-Observer). Thirdly, working in the visible domain benefits from a better sensitivity of detectors. Finally, the density of solar spectral lines is larger in the visible, which gives us more possibilities on the spectral band.

From Eq. (13), the velocity sensitivity is optimized by maximizing the ratio $\gamma\Delta/\lambda$. However, the experience from SYMPA shows that, in practice, this condition is insufficient because the fringe contrast has to be large enough to compete with the contrast of photometric structures on Jupiter. Indeed, the contrast between cloud bands and belts can reach 30%, and canceling the photometric modulation of fringes (Eqs. 6, 7) with contrast lower than 0.5 % is extremely challenging. That is why the *Echoes* science team recommended a fringe contrast of several percent, ideally 5 %, more being almost impossible.

We explored the whole solar spectrum in the visible domain varying the central wavelength and the width of the filter. For a given spectral band, we calculated the OPD that optimizes the sensitivity, implying a maximization of the product $\gamma\Delta$. We found an optimum for a central wavelength near 520 nm where spectral lines are thin and uniformly spaced, providing a good superposition with the interference fringes (Fig. 3). Larger spectral bandwidths increase the number of photons but reduces the fringe contrast. The best tradeoff was obtained with a central wavelength of 519.64 nm, a bandwidth of 1.07 nm and an OPD of 5023 μm. Operating parameters are determined by considering real filter profile, provided by the manufacturer. This results in a theoretical fringe contrast of 5.1%. Figure 4 represents the fringe contrast as function of the OPD. In order to keep the fringe contrast larger than 95% of its theoretical value, an OPD variation of $\pm$ 50 μm is tolerable.

3. Instrumental design

3.1. Requirements

The two science goals - seismology and atmospheric dynamics - require different kind of measurement and precision. Seismology is a long term monitoring of periodic fluctuations of the velocity field. It only requires relative velocity measurements, and the objective is an integrated noise level of about 1 cm^2 s^{-2} μHz^{-1} in the range $[500, 4000]$ μHz, where oscillations are expected. To the contrary, atmospheric dynamics requires absolute velocity measurements for each pixel. The precision on the velocity measurement must be better than 20 m s^{-1} pixel^{-1} hour^{-1}, aiming at integrated measurements of the mean zonal wind as function of latitude, with a precision better than 1 m s^{-1} in one Jovian rotation. These requirements were fixed to provide the best scientific objectives within the constraints of a space mission, i.e. with limited mass, power and data transmission capacity. Given the oscillation frequencies, the seismology objective imposes a 1-minute time sampling, which limits the number of pixels of the detector and therefore the angular resolution, to keep the telemetry to Earth feasible. The atmospheric dynamics objective needs a high spatial resolution, which limits the size of the instrument, scaled by the entrance pupil size, and thus the number of photons.

The optical design is studied within four major constraints. Firstly, the pupil size is determined from the noise level requirements. The number of photons received on the detector is a function of the distance to the planet, dependent on the mission profile, as well as the filter bandwidth and the instrumental transmission. Secondly, the FoV relies on the mission profile and the ability to combine both seismology and atmospheric dynamics at different phases of the mission, e.g. seismology far from the planet and atmosphere close to it. Thirdly, specific optical glasses are necessary to resist to radiations. Fourthly, materials are chosen to ensure thermal stability of the interferometer.

We consider a mission scenario that was envisioned for the JUICE mission. The distance between the spacecraft and Jupiter is plotted in Fig. 5. Seismology program requires continuous observations with a phase angle less than 90°, with two or more consecutive observing periods of 10 days at a distance where the

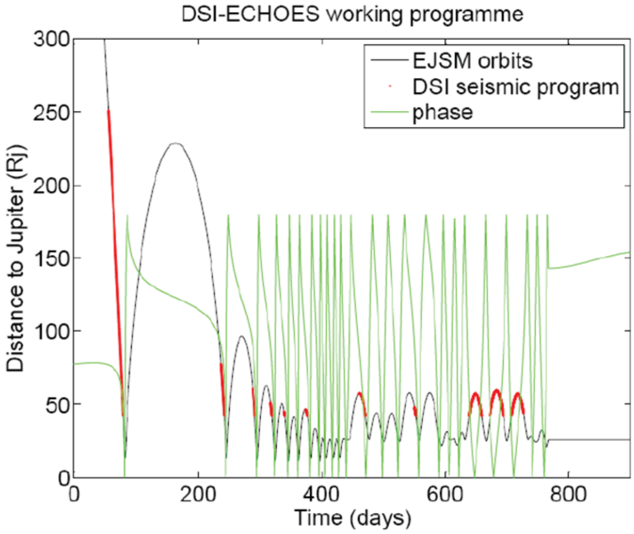

Fig. 5. Initial mission scenario. Best observing periods are in red, when apojove is greater than 42 R_j, and when the illuminated part of Jupiter can be continuously observed during more than 10 days.

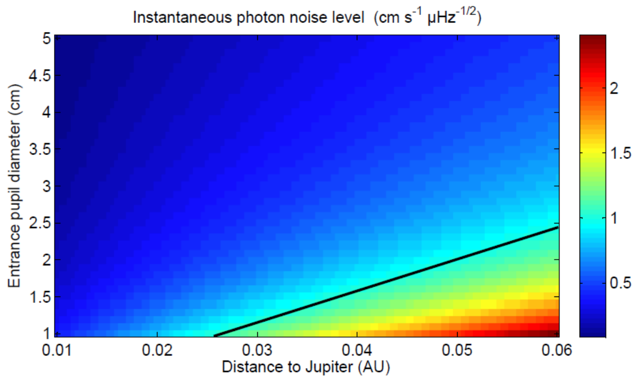

Fig. 6. Noise level on the velocity measurement, as a function of the input pupil diameter and of the distance to Jupiter. It gives the level in cms^{-1} that will be reached after 11 days of continuous observations.

whole planet disk fits within the field of view. The maximum phase angle is 90°, to allow for unambiguous identification of oscillation modes in a spherical harmonics base.

3.2. Pupil diameter and field of view

To design the instrument, we assume that precision is dominated by the photon noise, and we fix the error budget for the other noise contributions (jitter, thermal variation of the OPD, guiding noise) to be less than 50 % of the photon noise in the specified frequency range.

The pupil diameter depends on the distance to Jupiter. The number of photons coming from Jupiter as seen from Earth during planetary opposition, at a distance of r_0 = 4.2 AU, is $N_0 = 10^4$ photons Å^{-1} cm^{-2} s^{-1}. Thus, at distance r from the planet, it becomes:

$$N(t) = N_0 \left(\frac{r_0}{r(t)}\right)^2 \tag{14}$$

When taking into account the phase angle α under which the planet is observed, the photon amount is:

$$N(t) = N_0 \left(\frac{r_0}{r(t)}\right)^2 \frac{(1 + \cos\alpha)}{2} \tag{15}$$

By considering the total instrument transmission τ, the diameter D of the entrance pupil, the spectral bandwidth $\delta\lambda$ of the filter, and the exposure time δt, the total number of photons received by the spacecraft at a distance r is:

$$N(t) = \frac{\pi}{8}\, \tau\, \delta\lambda\, \delta t\, D^2\, N_0 \left(\frac{r_0}{r(t)}\right)^2 (1 + \cos\alpha) \tag{16}$$

The total instrument efficiency τ, including optical transmission, half-width filter transmission, and detector quantum efficiency, is estimated to be about 10 %.

The photon noise level on the velocity measurement is computed by combining Eqs. (16) and (13). Figure 6 displays the noise level as a function of the input pupil diameter, and the distance between the spacecraft and Jupiter, for a Jovian phase angle of 90°, which is the worst configuration for the seismology program. It arises that a noise level lower than 1 cm^2 s^{-2} μHz is always reached with a pupil diameter of 2 cm for a maximal observing distance of 0.05 AU. To take into account the other 50-% noise contribution, we choose a pupil diameter of 3.2 cm for the preliminary optical study. Note that if *Echoes* would observe from Earth, the pupil should be 200 times larger, i.e. a 6-m telescope.

The field of view also derives from the mission scenario. The minimal observing distance for the seismic program is set to 0.02 AU (42 R_J), implying of full FoV of 2.75°. This guaranties three periods of continuous observations longer than 10 days, and a total of possible observations of 70 days (over the two years duration of the Jupiter orbit phase of the mission) with a distance lower than 0.05 AU (∼ 100 R_J). It would actually be possible to increase the number of photons by reducing the minimum observing distance, but the atmospheric dynamics goal requires the best possible resolution on Jupiter to study small atmospheric features. In the considered scenario, a 2.75° FoV and a 1000 × 1000-pixel detector lead to a best resolution of 100 km on Jupiter at perijove (15 R_J).

3.3. Design of the Mach-Zehnder interferometer

The optical design of the Mach-Zehnder mainly results from the pupil size, the FoV, and the need to properly extract the fringe phase. About the latter, conditions are optimal if the fringes are straight, regularly spaced on the field, and sampled with at least 5 pixels per fringe. Obviously, the OPD must also respect the specification fixed in Sect. 2 and be stable in time.

Another important fact for designing the interferometer is the need for taking flat-field images, to calibrate both photometry and pixel response non-uniformity. Given the few space allowed on a spacecraft payload, we found a way to use the spectral calibration lamp as a flat field lamp. This is made possible by modulating the OPD fast enough to cancel out the fringes by shifting them of π several times during the exposure time. Thus, it imposes to place a device that has the capability of modulating the OPD.

The optical design presented on Fig. 7 answers to all of the above-mentionned requirements. Taking into account a minimal FoV of 2.75° and pupil diameter of 3.2 cm, **the optical quality of the instrument and Mach-Zehnder (CA VEUT DIRE**

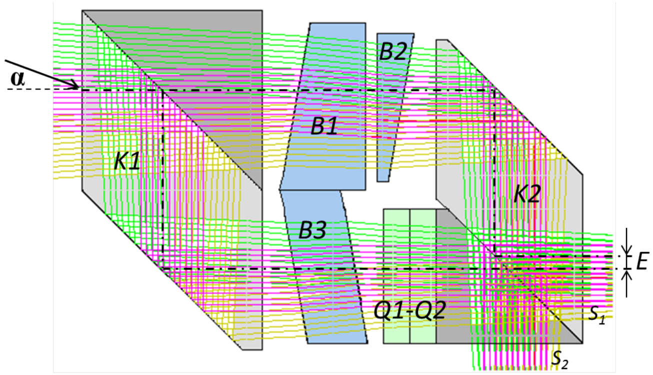

Fig. 7. Optical design of the Mach-Zehnder. Tilted plates are used to obtain straight fringes and to eliminate stray light. In the first arm, the B_2 plate is mounted on a titanium piezoelectric plate and achieves the OPD modulation. In the second arm, the Q_1 and Q_2 quartz plates perform the phase quadrature. The K_i blocks are in K5G20 and the B_i plates in BK7G18. S_1 and S_2 are the outputs of the interferometer and α is the FoV at the entrance of the Mach-Zehnder.

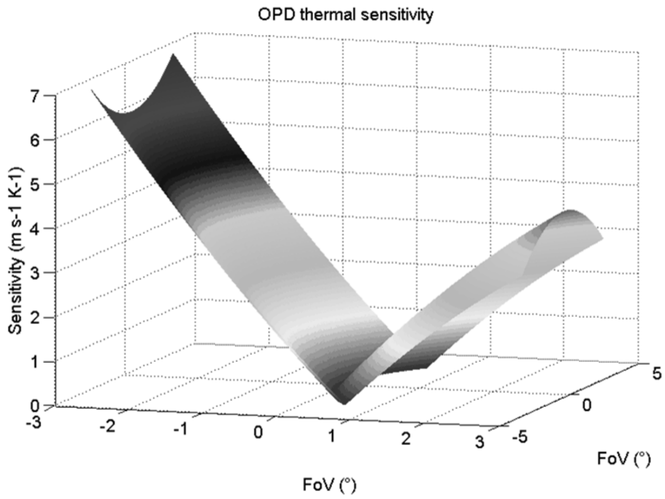

Fig. 8. The variation of the OPD thermal sensitivity is around 10 $m\ s^{-1}\ K^{-1}$ in the FoV.

QUOI ??), the optimal optical design leads to a field of the Mach-Zehnder itself of 3.9°. The image of the pupil inside the Mach-Zehnder has a 20-mm diameter. The OPD is the result of each optical element. The blocks K_1 and K_2 have a different size which induces a shift E between the two outputs beams and creates the main OPD. The tilted plates B_1-B_2 and B_3 are used to obtain straight fringes and to eliminate stray light. Note that B_1 and B_2 are separated in two prismatic components. This separation is used to place B_2 on a titanium piezoelectric plate and achieve the modulation of the OPD for calibrations. This modulation generates kπ/2 phase shifts of the interferometric fringes. In the second arm, the quartz plates Q_1 and Q_2 achieve the phase quadrature thanks to the orthogonal orientation of their optical axis.

We express the total OPD as function of the beam angles perpendicularly to the Mach-Zehnder entrance, α and β (β perpendicular to the plane of Fig. 7):

$$\begin{aligned}\Delta_{\text{total}}(\alpha,\beta) &= \Delta_{\text{empty}}(\alpha,\beta) + \Delta_{\text{Quartz}}(\alpha,\beta) + \sum \Delta_{\text{bk7}}(\alpha,\beta) \\ &= E\left\{\alpha + \sqrt{n_{\text{k5}}^2 - \alpha^2 - \beta^2}\right\} + e_Q(n_Q - 1) \\ &\quad + \sum e_{\text{bk7}}\{n_{\text{bk7}} \cos r - \cos i\} \qquad (17)\end{aligned}$$

where e is the thickness of the considered plate and n the refraction index of the considered material. The parameters i and r are respectively the angles of incidence and refraction of the incoming beam on the BK7G18 plate. They are given by:

$$n_{\text{bk7}} \cos r(\alpha,\beta) = \sqrt{n_{\text{bk7}}^2 - \sin^2\theta - \alpha^2 \cos 2\theta - \beta^2 \cos^2\theta + \alpha \sin 2\theta \sqrt{1 - \alpha^2 - \beta^2}}$$

and

$$\cos i(\alpha,\beta) = \alpha \sin\theta + \sqrt{1 - \alpha^2 - \beta^2}\ \cos\theta$$

where θ is the tilt angle of the plate. In order to maintain the required fringe contrast **(Table 1 D'où sort cette table et son contenu jamais présentés ???)**, the variation of the OPD (due to errors on glass plate thickness for example) must be less than $\pm 10\ \mu$m from the theoretical value.

The choice of the optical glasses respects two conditions. First, glasses must be resistant to spatial radiations. Secondly, they have to compensate for the variations of the refraction indices and for the thermal expansion in order to stabilize the OPD. Two glasses from Schott meet these conditions: BK7G18 and K5G20. The optical design will not be impacted by the received dose of radiations during the mission, in terms of refraction index variations or transmission variations **(REF ?)**. As regards temperature, the thermal sensitivity S of the OPD in the FoV (α, β) between two temperatures T_1 and T_2 is given by:

$$S(\alpha,\beta) = \frac{\Delta(\alpha,\beta,T_1) - \Delta(\alpha,\beta,T_2)}{\Delta(\alpha,\beta,T_0)}\ \frac{c}{\Delta T} \qquad (18)$$

where T_0 is the operating temperature, fixed at 20° C and $\Delta T = T_2 - T_1$. The calculation of the thermal sensitivity takes into account coefficients of thermal expansion (CTE) and variation of refractive index as a function of temperature, for each material. The optical design, sized by these parameters, is conceived in order to obtain $S = 0$ at the center of the FoV, by considering nominal values of the CTEs. Then we verify the variation of the thermal sensitivity in the whole FoV. Indeed, the OPD thermal sensitivity is directly linked to the velocity thermal sensitivity which must be less than 10 m s^{-1} K^{-1} across the FoV. We can see on Fig. 8 that the specification is respected.

3.4. Thermal effects

3.4.1. Mach-Zehnder interferometer

It is necessary to quantify the effects of probable manufacturing defects on the Mach-Zehnder performance. We studied the impact of uncertainties on the refraction indices, the thicknesses, and the material CTEs provided by manufacturers, as well as the effect of a beam tilt produced by a component prismatic error or a mispositioning. It arises that errors on thicknesses or tilts do not impact the performance because they can be compensated by an adjustment of the mobile plate B_2 in translation or rotation. However it is absolutely impossible with such a standard way to compensate for defects caused by the uncertainties on the CTEs. A variation of only few percents with respect to theoretical values significantly increases the thermal sensitivity of the Mach-Zehnder. Since **existing experimentations (de quoi ?**

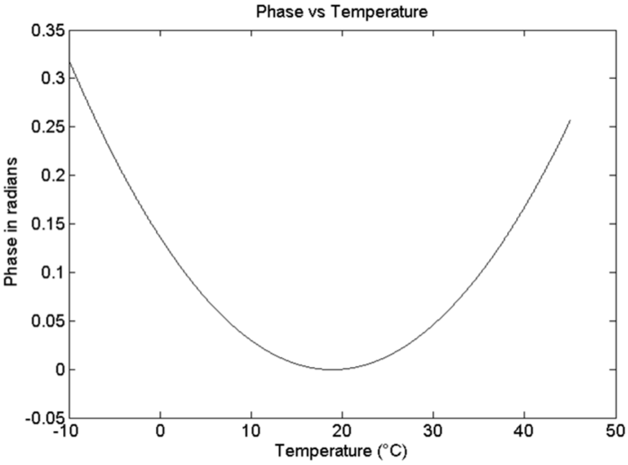

Fig. 9. The fringe phase has a quadratic variation in function of the temperature.

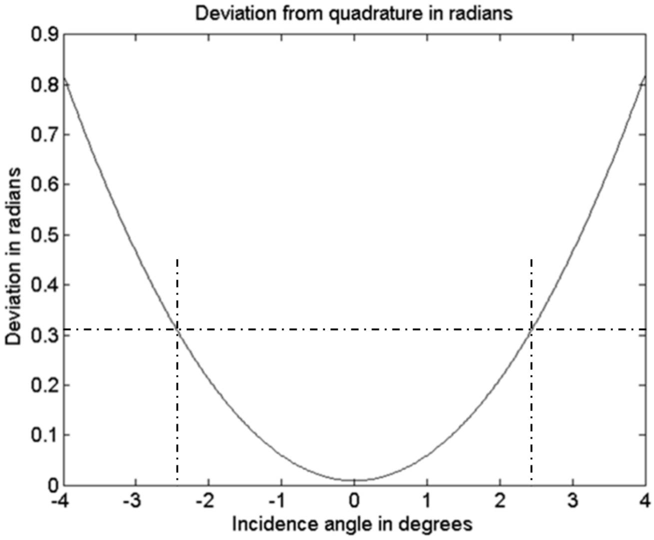

Fig. 10. Deviation from quadrature at the output of the quarter-wave plate. The specification on the phase quadrature (18° = 0.31 rad) is respected for a FoV of ±2.4°.

industrielles?) do not reach the required precision for the CTEs measurement, we need to define a protocol to determine the ideal parameters of the Mach-Zehnder.

The original process is based on the knowledge of the thermal behavior of the Mach-Zehnder. Figure 9 displays the dependence of the mean phase of the interferogram as function of the interferometer's temperature, which results to be quadratic. Simulations highlight a specific temperature value at which the phase variation is minimal, corresponding to the best thermal stability of the instrument. We call this particular value the *stability temperature*, equal to 19°C with CTEs at their nominal values. A departure to nominal values would shift the stability temperature. That is why we need to define a process allowing the modification of the stability temperature to be within a range which can be regulated, while ensuring nominal OPD.

Simulations show that plate thicknesses are directly related to the stability temperature. Therefore, it is possible to reach the required stability temperature value by adjusting the thicknesses of BK7G18 plates. Such a modification impacting the OPD, an adapted modification of the quartz plate thicknesses will overcome the effect, thanks to the low thermal dependence of the crystal. In conclusion, whatever the CTE values are, it is possible to modify the stability temperature value while ensuring the nominal OPD value.

Experimentally, the phase is measured at several stabilized temperatures. A quadratic fit of the measured curve provides the experimental stability temperature value. From this value, we will determine plate thickness improvements allowing to reach nominal parameters, i.e. a stability temperature of 19°C and an OPD of 5023 μm. Protocol and experimental results are detailed in Section **??**. **[Je ne comprends pas un truc: on veut s'arranger pour rester a 19 degres coute que coute, meme si les CTE ne sont pas nominaux, en faisant varier la taille des quartz, ou alors on se placera a la stability temperature correspondant aux vrais CTE? Eclaircir ce point dans les 3 precedents paragraphes.]**

3.4.2. Entrance Interferential filter

The thermal sensitivity is also affected by the presence of the spectral filter due to the temperature dependence of its central wavelength λ_0. This dependence is given by:

$$\lambda_{0(T)} = \lambda_0 + \xi \Delta T \tag{19}$$

where T is the temperature and $\xi = 1.6\ 10^{-5}\ \mu$m K^{-1} is the thermal variation coefficient of the filter. This results in a variation of the thermal sensitivity by less than 2.5 m s^{-1} K^{-1} in the FoV. The filter will have no impact on the Mach-Zehnder thermal sensitivity if it is regulated in temperature. Since the temperature fluctuations of the laboratory room are of several degrees, the filter must be placed in the vacuum chamber. **[Je doute qu'on aie deja parle de vacuum chamber.]**

3.5. Limitation of the Field of View

The FoV is limited by both the quarter-wave plate and the interferential filter.

Quartz is a birefringent material, with uniaxial anisotropy. Light with linear polarizations parallel and perpendicular to the material optical axis has unequal indices of refraction, denoted n_e and n_o. The incident light therefore splits into two linearly polarized beams, known as ordinary and extraordinary. In the Mach-Zehnder, two plates of quartz with perpendicularly optical axes are stuck together to achieve a quarter-wave plate, which creates a 90° phase shift between both polarizations. A departure to the quadrature between ordinary and extraordinary waves at the output of the quarter wave plate must be less than 18° (0.31 radians) in the FoV to ensure a contrast loss less than 5 % (Eq. 32). Figure 10 displays the deviation from quadrature in the FoV for $\beta = 0°$. Specification of 18° is respected for a FoV of ±2.4°. As expected, the difference to the quadrature is null when $\alpha = 0°$. According to this result, the useful FoV of DSI-Echoes is ±2.4°. We recall that the initial FoV of DSI was taken at ±3.9° (Section 3.2).

On top on the temperature dependence (Section 3.4.2), the central wavelength λ_0 of the filter depends on the angle of incidence α, such that:

$$\lambda_{0(\alpha)} = \lambda_0 \sqrt{1 - \left(\frac{n_e}{n}\right)^2 \sin^2\alpha} \tag{20}$$

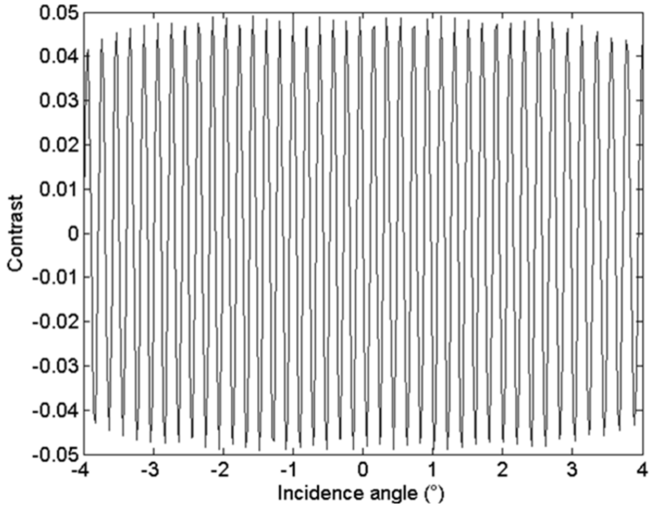

Fig. 11. Fringe contrast according to the incidence angle at the filter entry. Because the central wavelength of the filter depends on the angle of incidence, a loss of contrast occurs in the edges of the FoV.

where the refractive index of the filter is $n_e = 2.05$ and the refractive index of the environment equals to $n = 1$. The fringe contrast obtained by considering Eq. (20) is represented on Fig. 11. We note a loss of contrast of 15% at the edges of the FoV. Specification are respected for a FoV of ±3.5°.

To conclude, the quartz plates and the interferential filter impact the performance in terms of thermal sensitivity and FoV. The effects induced by the interferential filter are low. The quarter-wave plate is the main limitation. For the prototype study, we choose a FoV of ±3 degrees ensuring the minimal required FoV (Section 3.2) and the required fringe contrast. Such a value does not respect the somewhat arbitrary specification on the phase quadrature, but it is more than sufficient for the prototype study.

4. Real performance on a test bench

4.1. Implementation of the test bench

The experimental study of the Mach-Zehnder interferometer consists in measuring its real performance and adjusting it. Firstly, to meet the theoretical fringe contrast, we must control the wavefront quality, the transmission ratios between interfering beams, and the parallelism of the output beams. Then, to ensure a RSB loss equivalent to a contrast loss of 5%, we need to measure the transmission of each channel and the phase quadrature. Finally, to guarantee an OPD stability better than 16 pm rms, the stability temperature has to be precisely measured, and the choice of the piezoelectric plate must respect a specific position precision. The latter requires placing the Mach-Zehnder in a vacuum tank regulated in temperature, to avoid OPD variations due to the pressure.

We established an initial set of specifications, which are listed in Table 1. These values are initial guesses of what would be required to respect the total noise budget of the real instrument. Hence, they should not be regarded as strict acceptance conditions, but as guidelines for the realization of the prototype. A dedicated test bench has been implemented at the OCA, as well as the development of a software for image acquisition and commanding the elements of the test bench: detector, piezoelectric plate and cooler.

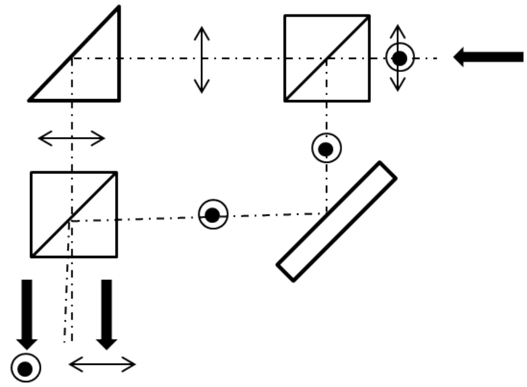

Fig. 12. The polarizer block is composed of a mirror, a prism and two polarizer cubes. A tilt is applied on the mirror to separate the images.

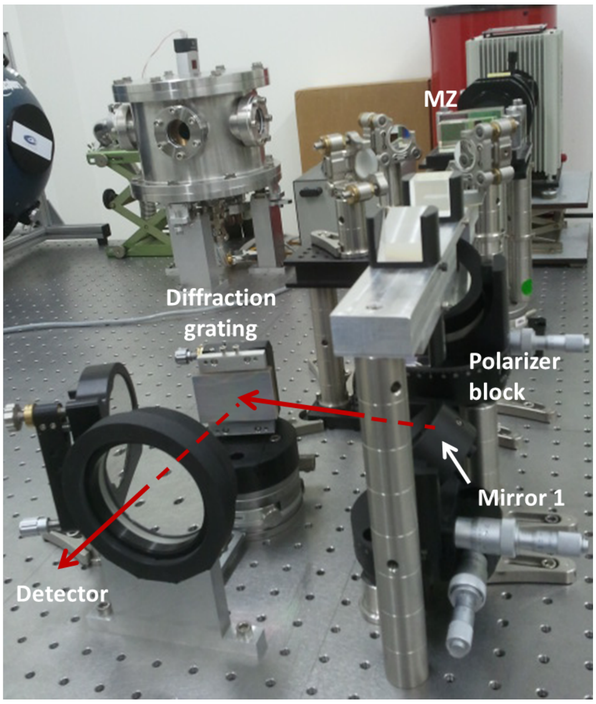

Fig. 13. The light source is injected in the Mach-Zehnder and then travels through the polarizer block. The light is directed to the diffraction grating (or a mirror) before arriving on the detector.

The test bench is composed of the following components, by following the light path: the light source, an adjustable slit, the Mach-Zehnder, the polarizer block (Fig. 12), the diffraction grating, the interferential filter and the detector. Depending on the desired measurement, the light source can be either a white light source, a spectral source, a laser, or the solar light. The polarizer block (Fig. 12) is composed of two polarizing beamsplitter cubes, a prism, and a mirror. It decomposes the incoming beam into its perpendicular and parallel components. The introduction of a tilt on the mirror separates the two images to get them side by side on the detector. After the polarizer block, the light is dispersed by the diffraction grating and then travels throughout the filter to the detector (Fig. 13). The dispersion of the diffraction grating is used for the OPD determination. After the adjustment of the OPD, the diffraction grating is removed and replaced by a mirror. Several configurations are possible depending on the needs.

Table 1. Specifications

	Name	*Specification*
1.	**Contrast loss**	**< 5%**
1.1	Transmission ratios	< 47.5%
1.2	Wavefront quality	130 nm ptv (λ/4 @ 519.64 nm)
1.3	Parallelism	< 2”
1.4	Optical Path Difference	5023 μm ± 50 μm
2.	**RSB loss**	**Equivalence in contrast loss**
2.1	Intensity differences	< 30%
2.2	Phase quadrature	90° ± 18°
3.	**OPD stability**	**16 pm rms**
3.1	Mobile plate stability	π/300 (0.9 nm)
3.2	Stability temperature	19° C ± 0.3° C

4.2. Adjustment of the OPD

For all the tests, it is crucial to measure the actual OPD. We do so by measuring the fringe number in the FoV with white dispersed light. It requires to determine the dispersion of the grating, the method consisting in imaging the solar spectrum on the detector and locating the position of the reference spectral lines (`http://bass2000.obspm.fr/solar_spect.php`). The design is conceived to produce 20 fringes between two reference wavelengths, given by $\Delta\lambda = \lambda_2 - \lambda_1$ (see Fig. 3), for the nominal OPD value of 5023 μm, such that :

$$\Delta\left(\frac{1}{\lambda_1} - \frac{1}{\lambda_2}\right) = 20 \tag{21}$$

However it is important to consider the chromatic dispersion **[of what ?]**, because the OPD is a function of wavelength, through the refraction indices of the prisms. The fringe envelope corresponds to the module of the Fourier transform of the incoming spectrum. In an environment other than air, chromatic dispersion affects the result, as illustrated by Fig. 14. Considering the correction **[“the correction”, quelle correction ? Obscur]**, the OPD value Δ is given by **[Il y a un besoin d’expliquer mieux l’effet de la dispersion chromatique. Dire mieux de quoi on parle et de comment eJan a obtenu la correction. C’est impigeable tel quel]** :

$$\Delta = \frac{\lambda_1\lambda_2 N_f}{N_{pix} d} - \kappa\lambda_0$$

with N_f the number of fringes measured in the FoV, $N_{pix} = 1024$ the number of pixels on the detector, d the measured dispersion and κ the chromaticism correction, determined by simulation **[En quoi consiste cette simulation?]**.

Raw experimental fringes are presented Fig. 15. The fringe number is deducted from the position of the Fourier transform fringe peaks of the acquired image. The resolution is improved by using the zero padding method **[Ref?]**, allowing a fringe number determination with a precision of 0.06 fringe.

We determine the OPD value at an arbitrary position of the mobile plate B_2. If the measured OPD does not respect the specification (Table 1), the value is modified by translating the B_2 mobile plate. Finally, we have adjusted the Mach-Zehnder at its nominal OPD, i.e. 5023 μm. Because the precision on the dispersion measurement is 7.10^{-6} nm pixel^{-1}, the precision on the OPD determination is ± 11 μm, allowing the specification compliance. The value being adjusted, the next step consists in measuring the fringe contrast.

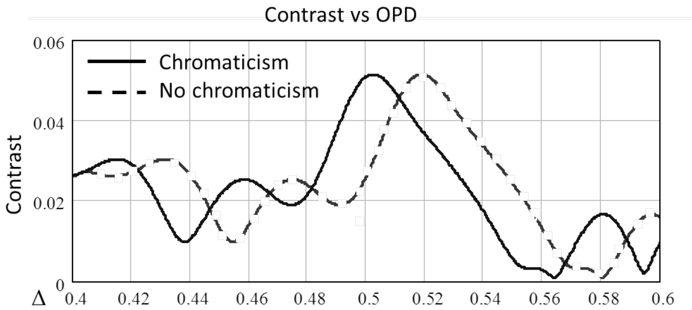

Fig. 14. Fringe contrast as a function of the OPD, with and without chromatic effect. Optimal contrast is obtained for an OPD of 5200 μm when considering chromatic dispersion. By correcting this effect, the optimum is obtained for an OPD of 5023 μm (Jean Gay **[quoi Jean Gay?]**).

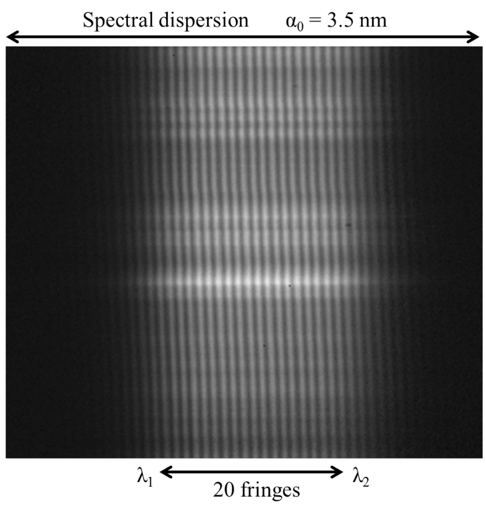

Fig. 15. Raw experimental fringes of the Mach-Zehnder obtained with a dispersed white light source. The number of fringes in the FoV provides the value of the OPD.

4.3. Fringe contrast

4.3.1. Sources of contrast degradation

Specifications require that the fringe contrast can be 5 % off with respect to its theoretical value. The contrast is affected by the

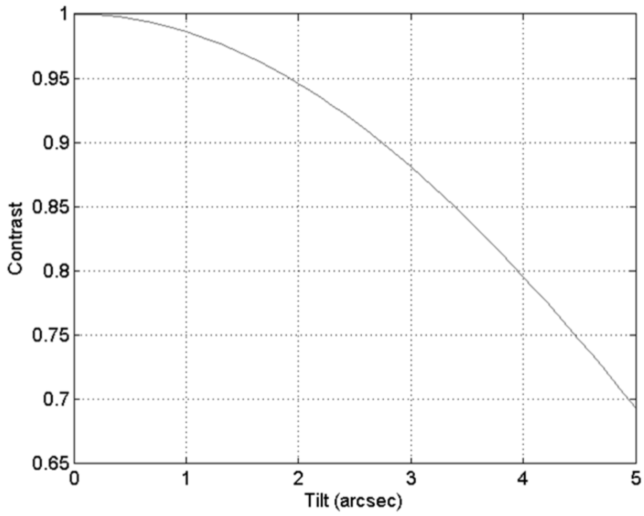

Fig. 16. Contrast as a function of differential tilt between pupils.

wavefront quality, the parallelism of the output beams, the transmission ratios between interfering beams, and the OPD adjustment.

The first step consists in adjusting the parallelism at the output of the Mach-Zehnder, which must be better than 2 arcsec to respect the specifications, (Fig. 16). In practice, the method we used leads to an adjustment precision of ±2.5 arcsec, which implies a loss contrast of 9 %. To improve the precision, a new mechanical solution could refine the adjustment, and a dedicated bench is needed to achieve such very high precision verification. This however goes beyond the scope of the present work.

The quality of the wavefront is measured thanks to a dedicated wavefront analyzer (SID4 from Phasics). The method consists in a differential measurement **[of what ?]** achieved with a white light source filtered at 519.64 nm. The measured wavefront is $\lambda/7$ peak-to-valley, which is much better than the specification and implies a loss contrast less than 1 %.

We then measure the transmission ratios between the outputs of the two arms of the interferometer for each polarization, i.e. between the interfering beams. From Table 1), the specification is $\leq$ 47.5 % **[Ca veut dire quoi ce 47%? 47% de quoi? Impigeable]**. The first arm with B_1 plate is noted v_1 and the second v_2. We express the contrast C **[Pourquoi plus gamma?]** of a considered output as function of the experimental transmission ratios ΔT **[d'ou ca sort?]**:

$$C = \frac{2\sqrt{\Delta T}}{1+\Delta T} \tag{22}$$

Results are **[Ce paragraphe est strictement impigeable. Results de quoi ? On s'y perd. Reecrire.]**:

$$\begin{aligned}
\Delta T_{s1\parallel} &= \frac{T_{v1s1\parallel}}{T_{v2s1\parallel}} = 0.936 \rightarrow C_{s1\parallel} = 0.999 \\
\Delta T_{s1\perp} &= \frac{T_{v1s1\perp}}{T_{v2s1\perp}} = 0.991 \rightarrow C_{s1\perp} = 0.999 \\
\Delta T_{s2\parallel} &= \frac{T_{v1s2\parallel}}{T_{v2s2\parallel}} = 0.513 \rightarrow C_{s2\parallel} = 0.947 \\
\Delta T_{s2\perp} &= \frac{T_{v1s2\perp}}{T_{v2s2\perp}} = 0.633 \rightarrow C_{s2\perp} = 0.974
\end{aligned} \tag{23}$$

Specification on the transmission ratios is not respected **[Ah bon ? Pourquoi, on voit ca d'ou?]**, due to the non-conformity of the semi reflective coatings. Indeed, transmission and reflection coefficients are respectively about 0.55 and 0.35, but are not dependent on the polarization **[Que nous dit ce "but are not dependent on the polarization"? Ca apporte quoi ? On en conclue quoi ? C'est bien, c'est pas bien, c'est voulu?]**. The consequence of such results is a degradation of the theoretical contrast up to 6 %.

4.3.2. Measured contrast

The fringe contrast is measured at each output of the Mach-Zehnder, for each polarization. The precise value can only be measured by using filtered solar spectrum. The protocol consists in determining the amplitude of the Fourier transform peaks of the image, such as : $C = (2A_1)/A_0$, where A_0 and A_1 indicate the amplitudes of the central and of the fringe peaks. It results:

$$\begin{aligned}
C_{s1\parallel} &= 4.3\% \\
C_{s1\perp} &= 4.2\% \\
C_{s2\parallel} &= 3.9\% \\
C_{s2\perp} &= 4.1\%
\end{aligned} \tag{24}$$

The specification is thus not respected. This contrast loss ranges from 16 % to 22 %, which generates a rise of the noise level of about 20 %.

The observed loss of contrast is caused by residual transmission ratios, OPD and parallelism misadjustments, and wavefront quality error. Because the measurement was obtained at an actual OPD of 5073 μm instead of 5023 μm, a loss contrast of 5% is induced (Fig. 4). The total contrast is the product of:

$$C_{\mathrm{tot}} = C_{\Delta T}\, C_{\parallel}\, C_{\mathrm{WFE}}\, C_{\mathrm{OPD}} \tag{25}$$

Depending on the output, the evaluated contrast loss is between 14% and 19%. It corresponds to the experimental values, by considering the measurement precision of 4 % **[D'ou ca sort ce 4% ?]**.

4.4. Signal-to-noise ratio

The SNR is affected by any photometric unbalance between the four outputs at each output, and a departure with respect to the phase quadrature. The objective is to keep it within 5 % of its nominal value.

On top of a contrast loss, optical transmission affects the SNR. To get an SNR loss lower than 5%, the difference between the intensities of each channel must be less than 30 %. The measures intensities at each output are:

$$\begin{aligned}
T_{s1\parallel} &= 0.846 \\
T_{s1\perp} &= 0.854 \\
T_{s2\parallel} &= 0.899 \\
T_{s2\perp} &= 0.859
\end{aligned} \tag{26}$$

The maximal intensity difference is 5.3%, which means that the specification is respected.

Regarding phase quadrature, the theoretical phase shift of the interference fringes is π between the two outputs of same polarization and $\pi/2$ between the two polarizations of a given output. Let us indicate the phase shift between I_1 and I_2 as $\Delta\phi_1$, the phase shift between I_1 and I_3 as $\Delta\phi_2$, and the phase shift between I_1 and I_4 as $\Delta\phi_3$. We measure the phase of each interference pattern by first vertically collapsing the row of each

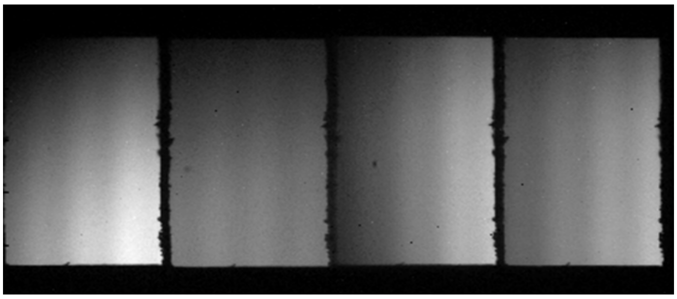

Fig. 17. Experimental solar fringes, obtained with filtered solar spectrum.

image to increase the SNR. The phase is determined by measuring the position of the Fourier transform of the average fringe, which allows for a measurement precision of 0.5°. We obtain:

$$\Delta\phi_1 = 90^\circ + 2.5^\circ \quad (27)$$
$$\Delta\phi_2 = 180^\circ - 0.23^\circ \quad (28)$$
$$\Delta\phi_3 = 270^\circ + 2.3^\circ \quad (29)$$

The departure to a perfect phase quadrature affects the velocity sensitivity of the instrument. If ε is the phase shift between U and V, we introduce the variables U' and V' defined by:

$$U' = \frac{U\cos\frac{\varepsilon}{2} - V\sin\frac{\varepsilon}{2}}{\cos\varepsilon} \quad (30)$$
$$V' = \frac{V\cos\frac{\varepsilon}{2} - U\sin\frac{\varepsilon}{2}}{\cos\varepsilon} \quad (31)$$

The new complex interferograms U' and V' are in phase quadrature, but the standard deviation on velocity measurements (Eq. (13) increases to:

$$\delta'_v = \frac{\delta_v}{\cos\varepsilon} \quad (32)$$

The SNR loss is thus less than 0.1%, considering the maximum quadrature phase error of 2.5°, which can be neglected.

4.5. Stability of the OPD

Both fluctuations of the mobile plate and of the stability temperature may affect the OPD stability.

4.5.1. Mobile plate

During calibration processes, OPD modulation is achieved by using the translation of the mobile plate mounted on the piezoelectric plate. The aim is to phase-shift the fringes of $k\pi/2$ to interchange images on the detector. In order to not introduce noise, the piezoelectric plate must respect a position precision **[de combien?]**. Studies based on simulations **[develope un peu, elles consistent en quoi ces simus]** lead to a position precision of $\pi/300$, i.e. 0.9 nm. **[Et c'est OK ca? Si oui dis le.]**

4.5.2. Stability temperature

The thermal sensitivity of the Mach-Zehnder is related to its operating temperature. To ensure a thermal sensitivity less than 10 m s^{-1} K^{-1} on the FoV, the interferometer must be regulated at ±0.3°C around the theoretical stability temperature.

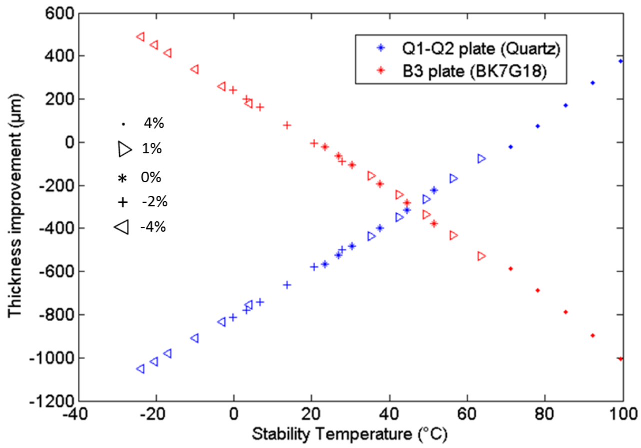

Fig. 18. Thickness corrections to be made on the Q_1 - Q_2 and B_3 plates in function of the stability temperature. Each symbol corresponds to a different error on the quartz and BK7G18 coefficient of thermal expansion. For each error on the quartz coefficient, given by the figure legend, a variation between -4% and +4% on the BK7G18 coefficient is achieved.

As explained in Section 3.4.1, the thermal stability of the Mach-Zehnder is optimal when regulated at the judicious temperature. Theoretical simulations show the possibility to modify the stability temperature while ensuring the nominal OPD. However the results are only valid if the CTEs are nominal. Since the CTEs are unknown, the protocol must be revised. Figure 18 represents the improvements to be done to the plate thicknesses as a function of the measured temperature. Simulations are made for an arbitrary OPD value of 5213 μm. Each symbol corresponds to a different error on the quartz or BK7G18 coefficient of thermal expansion. It appears that regardless of CTE errors, the plate thickness modifications are always linear relatively to the measured temperature **[pas super clair]**.

Measuring the stability temperature requires to determine the fringe phase with the best precision. For this, we used a specific configuration of the test bench. To get rid of the diffraction grating, we used a monochromatic source, composed of a Cadmium spectral lamp placed before the interferential filter. The working wavelength is 508 nm instead of 519 nm, which impacts the value of the stability temperature. Using this wavelength shifts the stability temperature of 2.4°C. Since the stability temperature is a function of wavelength, as is the OPD, the Mach-Zehnder is placed in the vacuum tank with a temperature regulation precision of ± 0.1°C. Preliminary acquisitions emphasized the necessity to turn on the spectral lamp few hours before the beginning of the measures. For each acquisition, the temperature has been stabilized during 24 hours.

Again, to measure the phase with high precision, the images are vertically collapsed and the phase is measured from its Fourier transform. The measurement accuracy is limited by the knowledge on the relative positions of each image on the detector, which is mandatory for comparing the mean phase from an interferogram to another. A relative position precision of 0.1 pixel induces to a phase shift error of 1.4 mrad, corresponding to a velocity error of 7 m s^{-1}. This bias is *a priori* constant and can be calibrated.

The procedure is applied for four different stabilized temperatures. Figure 19 represents the measured phase as function of the Mach-Zehnder temperature, for a working wavelength of 508 nm and an OPD of 5073 μm. The measured stability tem-

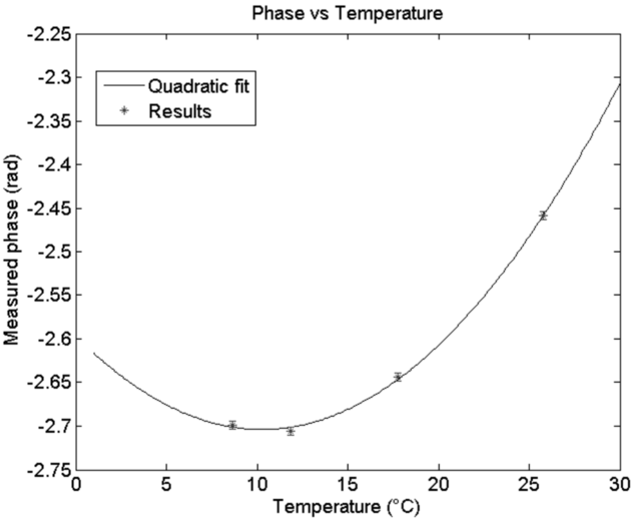

Fig. 19. Measured phase in function of the Mach-Zehnder temperature. We observe a stabilization around 10° C.

perature deduced from a quadratic fitting is 10.3°C ± 0.4°C. It corresponds to a working stability temperature of (12.7 ± 0.4)°C at the nominal wavelength. The measurement precision implies an increase of the thermal sensitivity in the FoV of 1 m s^{-1} K^{-1}. So the variation of the thermal sensitivity is 11 m s^{-1} K^{-1} in the FoV, i.e. a noise level less than 1.1 m s^{-1}, if thermal variations are less than 0.1 K.

The variation of the stability temperature is linear as a function of the OPD. Simulations predict a stability temperature of about 3°C for the nominal OPD value **[phrase pas claire du tout. 3 degres pour quoi faire ? Pour revenir a l'opd theorique?]**. This is the reason why we prefer to work at the OPD value of 5073 μm, implying a contrast loss of 5 %, but avoiding thickness improvements. Such a result implies to work at the determined temperature value of 12.7°C. Considering the future project of observations with the prototype, we plan to install it at the focus of a telescope during winter 2014. At this season, the room temperature will be closer to 12.7°C than 19°C, implying an optimal temperature regulation at the determined value. That is why we have decided to keep the current prototype configuration, without improving plate thicknesses to reach the nominal stability temperature. The Table 2 summarizes the experimental results. Initial specifications on contrast loss and stability temperature are not respected.

5. Discussion and conclusions

From the test bench experiments, we are able to draw conclusions on the instrument design and actual performance. The loss of contrast leads to an increase of the noise level of about 20 %. We recall that for the nominal OPD value of 5023 μm, the contrast would be better than 5 %, i.e. a loss contrast between 11% and 17%. To overcome the loss contrast, the entrance pupil diameter could be increased, to receive more photons. Besides, the measured stability temperature does not correspond to the expected value. However the Mach-Zehnder regulation can be achieved at any temperature in the thermal regulation range defined by the cryothermostat, with no impact on the thermal sensitivity in the FoV. We have demonstrated the possibility to measure precisely the phase, which provides an accurate stability temperature determination. From this temperature, the optimal thermal stability is ensured despite the ignorance of the CTEs. But results have been obtained by considering the whole FoV. That is why the last step of the study will consist in measuring fringe phase at each point of the four images.

The main objective of the DSI *Echoes* is to detect the oscillation modes of Jupiter with amplitudes of 1 cm s^{-1} in a frequency range between 500 and 4000 μHz. It requires a noise level in this range less than 1 cm^2 s^{-2} μHz^{-1} and a duration of observations of about 50 days. For a typical mission scenario, a lower photon noise level can be achieved, as proved by the study. It implies that the other noise sources are lower than this level. We have seen on the prototype that the fabrication process does not compromise the noise budget. The total decrease in SNR is less than 20 % and this could be improved by a better control of the parallelism of the pupil inside the Mach-Zehnder. Thermal variations have been carefully taken into account in the study, and we have demonstrated that they can be less than 11 m s^{-1} K^{-1} across the FoV. It corresponds to a noise level of 1.1 m s^{-1}, if thermal variations are less than 0.1K.

In order to keep the noise budget within the scientific requirement, it is necessary to have a precise knowledge of a given number of instrumental parameters. The critical parameters for the velocity measurement are: OPD, distortion between images, detector response, photometry, contrast and phase at any point of the images. The raw measurements have to be converted in intensity, polarization and phase measurement. That is why they must be derived from the calibration. On ground, initial parameter values are determined. In space, we expect a calibration procedure at the beginning of the observations. Other calibration phase might be required depending on the stability of these parameters. That is why the calibration process will be studied on the test bench, using the OPD modulation. It is possible to reduce the effects of the pixel sensitivities to a level less than 10 m s^{-1} $pixel^{-1}$ thanks to a dedicated calibration process. Because these errors are constant over time, they can be estimated directly on the data.

Experimental measurements achieved in laboratory are not representative of the performance that can be obtained in spatial conditions. For example, the detector used for the tests was not thermally controlled, and the calibration of the pixel sensitivities has not been made. Measurement dispersion, for acquisitions shorter than 1 hour, is dominated by detector and numerical noise. This was sufficient to demonstrate the dependance of the phase with the temperature in the lab. The precision can largely be increased. Considering these conditions, measured dispersion is 0.1 mrad for acquisitions every minute during 100 minutes, corresponds to a noise level of 4 cm^2 $s^{-2}\mu Hz^{-1}$ in a frequency range of 1500 μHz. In better operating conditions, no doubt that we will reach results comparable to specifications in laboratory.

Finally, to validate the instrumental concept, the prototype will be placed at the focus of a telescope to observe Jupiter in real conditions. It requires defining upstream optics to adapt the FoV. The tests will be performed with the 1.5-m MeO telescope at Calern Observatory (France). First observations will take place in January 2014.

The studies of *Echoes* are therefore confirmed by the experimental results, and no elements susceptible to compromise the operation in a spatial environment have been identified. *Echoes* is a new concept of spatial instrument, designed to provide innovative measurements in planetology in general, and for the internal structure of giant planets more particularly. In this paper, we have demonstrated the application of the concept to seismology of Jupiter, in the frame of space mission to this planet. Obviously, it can be adapted to other giant planets, for which

Table 2. Experimental results summary

	Name	*Specification*	*Result*	*Conformity*
1.	**Contrast loss**	< 5%	20%	No
1.1	Transmission ratios	< 47.5%	48.7%	Yes
1.2	Wavefront quality	130 nm ptv (λ/4 @ 519.64 nm)	λ/7 @ 519.64 nm	Yes
1.3	Parallelism	< 2”	2.5”	No
1.4	Optical Path Difference	5023 μm ± 50 μm	5073 μm ± 11 μm	Yes
2.	**RSB loss**	Equivalence in contrast loss	1%	Yes
2.1	Intensity differences	< 30%	5.3%	0.9%
2.2	Phase quadrature	90° ± 18°	90° + 2.5°	0.1%
3.	**OPD stability**	16 pm rms	VALUE	??
3.1	Mobile plate stability	π/300 (0.9 nm)	π/850 (300 pm)	Yes
3.2	Stability temperature	19° C ± 0.3° C	12.7° C ± 0.4° C	No

space mission are presently envisioned (Hofstadter et al. 2013; Schmider et al. 2013). It is also possible to adapt this instrumental principle to other fields to measure velocity maps. It concerns particularly solar physics and planets atmosphere dynamics (giant planets, Venus, Titan). Another possible application would be the detection of pollutant in the Earth atmosphere, for instance. This could be done by measuring the contrast of the fringes in daylight scenes.

Acknowledgements. The authors thank the Centre National d’Etudes Spatiales (CNES) and Thales Alenia Space (TAS) for the thesis funding, and CNES for the Mach-Zehnder R&D support.

References

Bercovici, D. & Schubert, G. 1987, Icarus, 69, 557
Cameron, A. G. W. 1978, Moon and Planets, 18, 5
Christensen-Dalsgaard, J. 2004, Sol. Phys., 220, 137
Deming, D., Mumma, M. J., Espenak, F., et al. 1989, ApJ, 343, 456
Deubner, F.-L. 1975, Sol. Phys., 40, 333
Gaulme, P., Schmider, F.-X., Gay, J., Guillot, T., & Jacob, C. 2011, A&A, 531, A104
Gaulme, P., Schmider, F. X., Gay, J., et al. 2008, A&A, 490, 859
Gudkova, T. V. & Zharkov, V. N. 1997, Solar System Research, 31, 99
Hofstadter, M. D., Murphy, N., Matousek, S., et al. 2013, in AAS/Division for Planetary Sciences Meeting Abstracts, Vol. 45, AAS/Division for Planetary Sciences Meeting Abstracts, 211.24
Jackiewicz, J., Nettelmann, N., Marley, M., & Fortney, J. 2012, Icarus, 220, 844
Mayer, L., Quinn, T., Wadsley, J., & Stadel, J. 2002, Science, 298, 1756
Mosser, B., Maillard, J. P., & Mékarnia, D. 2000, Icarus, 144, 104
Mosser, B., Mekarnia, D., Maillard, J. P., et al. 1993, A&A, 267, 604
Safronov, V. S. & Ruskol, E. L. 1982, Icarus, 49, 284
Schmider, F.-X., Fossat, E., & Mosser, B. 1991, A&A, 248, 281
Schmider, F. X., Gay, J., Gaulme, P., et al. 2007, A&A, 474, 1073
Schmider, F.-X., Mousis, O., Fletcher, L. N., et al. 2013, in SF2A-2013: Proceedings of the Annual meeting of the French Society of Astronomy and Astrophysics, ed. L. Cambresy, F. Martins, E. Nuss, & A. Palacios, 65–69
Vorontsov, S. V., Zharkov, V. N., & Lubimov, V. M. 1976, Icarus, 27, 109
Wyant, J. C. 1975, Appl. Opt., 14, 2622